High Integrity Multi-Sensor Navigation System For Safety Critical Applications

M. Saidani, D. Gallego Maya, A. Guinamard

SBG-Systems SAS - 1 avenue Eiffel - 78420 - Carrières-sur-Seine - France

KEY WORDS

Integrity Monitoring, GNSS, INS, Odometer, Tightly Coupled Data Fusion, RTK, ARAIM, FDE, PL.

ABSTRACT

The high increase of safety critical applications such as autonomous driving, Advanced Driver Assistance System (ADAS), Intelligent Transportation System (ITS) and many applications that can cause human or economic losses pose a significant challenge of navigation integrity. Although the integrity concept is not new, a major challenge in these applications is to ensure both high accuracy and high integrity in very challenging environments. In response to the high requirements of these applications, this paper will present a high integrity multi-sensor navigation system specially designed for safety critical applications. The system is composed of a MEMS Inertial Measurement Unit (IMU), a multi-constellation multi-frequency GNSS receiver and an odometer communicating via a CAN bus. A tightly coupled solution [1] based on an Extended Kalman Filter (EKF) has been developed by SBG-Systems to fuse all these sensors to deliver a high accuracy and availability especially in complex environments where satellites signals are prone to attenuation or even unavailability. In addition, advanced vehicle modeling and constraints [2] have been added with respect to the motion profile to provide a navigation solution for the targeted applications. The integrity management starts with the correction service such as the State Space Representation Corrections (SSR) [3]; many services now provide SSR corrections over the world with integrity messages. Another challenging aspect of robust navigation is the integration of an Advanced Receiver Autonomous Integrity Monitoring (ARAIM) [4], which can be defined as a two steps process. First, a Fault Detection and Exclusion (FDE) is performed, then if a consistent solution is found the Protection Levels (PL) are calculated [5]. The system will assure a continuous monitoring of multiple integrity indicator, the PL will be computed and compared to an Alert Limit (AL) threshold to notify the user about system availability. During the GNSS outages, the INS and the odometer not only keep the precision of the position solution, but also scale and propagate the PL using the inertial models [6]. This paper also focuses on the integrity assessment of the developed system. Indeed, an extensive test campaign has been conducted to evaluate the maturity of the technology and its compliance with autonomous vehicles requirements. Several ranges of products and configurations are tested to measure the performance driving factors and evaluate the typical use case.

I. INTRODUCTION

The integrity monitoring and availability of a navigation system has been for the last decade one of the main subjects in the research community. Initiated with Safety of Life aviation applications, the GNSS integrity was designed using a combination of two major components. A ground or satellite based augmentation systems (SBAS or GBAS) are used to track satellites or constellations issues, and a receiver side integrity monitoring used to track the receiver specific errors like interference issues. Traditionally, the RAIM algorithm is used for that purpose, with the ability of detecting a single satellite fault. New land based applications face a major challenge with a lot of multi-path errors affecting the system performance while requiring a much higher precision than in the aviation field (typically targeting a lane level accuracy). It's then necessary to consider solutions that integrate more sensors to overcome these challenges: A high accuracy augmentation systems like SSR or RTK, a robust multi-fault ARAIM system, and the aid of external sensors like odometer, IMU and possibly perception sensors.

This paper will present a high integrity multi-sensor navigation system for safety critical applications, it will be structured as follows: the first section defines the principles of INS, GNSS and odometer data fusion. The second section introduces the notion of integrity applied to the multi-sensor navigation system, where the concept of detection and exclusion and protection level are detailed. Finally, the last section will illustrate the performance of the developed system for an automotive motion profile under three different scenarios: open sky, light urban and harsh urban.

II. MULTI-SENSOR NAVIGATION SYSTEM

The INS, GNSS and odometer data are commonly fused through the Kalman filter. The fusion of multiple sensors provides high precision of position, velocity, and attitude. The advantage of the multiple sensor fusion is that each sensor overcomes the drawbacks of the others. In fact, the GNSS provides measurements with a long-term absolute accuracy, typically with a low rate under 10 Hz, but the signals can be blocked or have a poor quality especially in harsh environments. An Inertial Navigation System (INS), including gyroscopes, accelerometers, and odometers in contrary has good short-term accuracy, but an overtime growing error due to integration of drift and noise. The INS has a high update rate, usually more than 100 Hz and a high availability. A combination of these systems has the possibility of providing a high bandwidth with both short and long term accuracy. In addition to the data fusion, an advanced dynamic modeling specific to the tracked vehicle is applied, which improves significantly the performances.

There exists a different method for fusing GNSS, INS and odometer data with each having its owns pros and cons. In this paper, we will be interested in a tightly coupled architecture, which proved its superiority over the loosely coupled solution, especially in the context of robust navigation. Using this architecture, the measurements from the GNSS receiver, IMU and odometer data are integrated at a deeper level in a single filter which overcomes the problems that could arise with colored noises. The pseudorange and the carrier phase measurements from the GNSS receiver are integrated with the IMU and odometer in the same filter as depicted in Figure 1

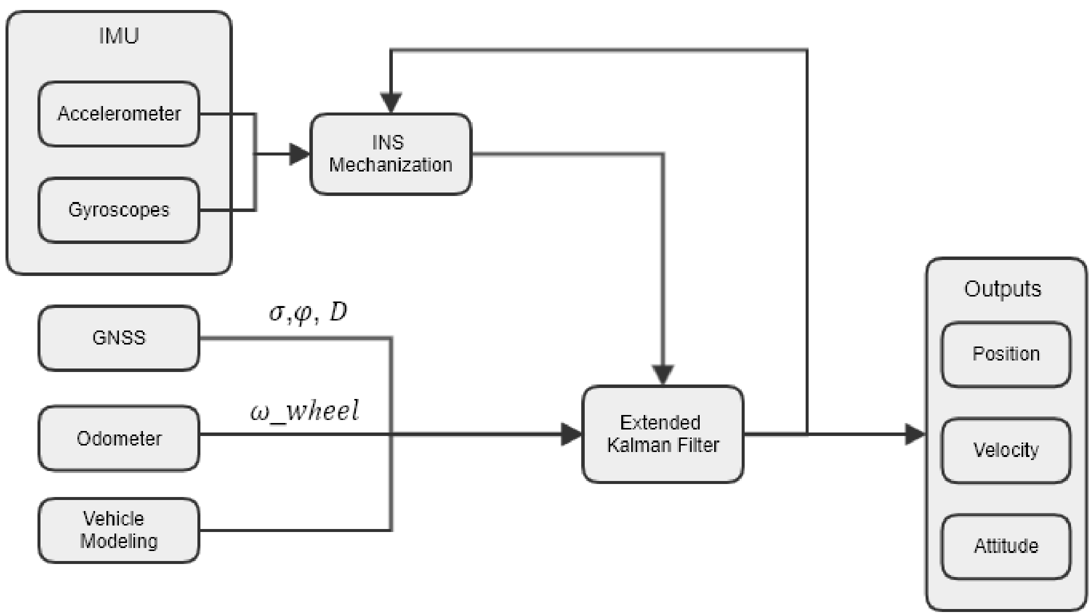

Figure 1: Tightly Coupled Architecture.

III. INTEGRITY

Integrity is defined as the measure of the trust that can be placed in the correctness of the information supplied by a navigation system. The aim of integrity monitoring is to provide timely warnings to users when the system results are abnormal or unavailable for navigation. This integrity can be achieved by using several complementary methods. For instance, using corrections services that include integrity monitoring such as SSR serve as a pre-validation step for GNSS signals, but such corrections don't overcome the receiver related errors such as multipath. To overcome the receiver errors, an ARAIM algorithm is developed in this paper. An ARAIM algorithm detects and removes the faulty observations, thanks to the Fault Detection and Exclusion (FDE) part. Once a consistent subset of observations is found, the protection levels are calculated to assess the quality of the calculated solution.

To evaluate the developed integrity algorithm, we will use the Stanford diagram (Figure 2) which is considered as the reference tool to evaluate such types of algorithms.

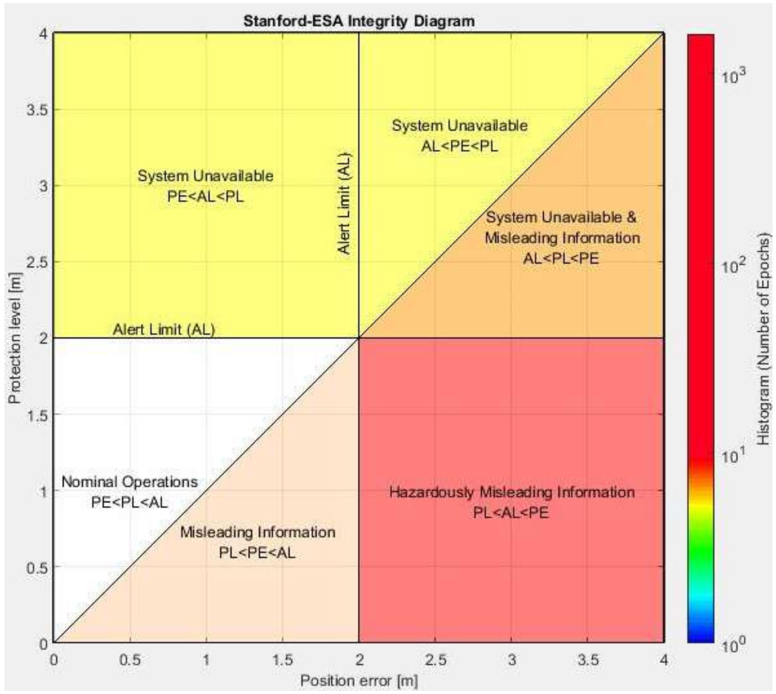

Figure 2: Stanford Diagram.

1. Navigation Engine

Figure 3 shows an overview of the navigation and integrity system. It is clear that the integrity plays a major role in each step of the process. In the first place, all the inputs are validated before entering the system. Then, the data from all the sensors is fused using an Extended Kalman Filter in an RTK tightly coupled architecture with INS data. At this stage we enter the RAIM/FDE block that oversees multiple complex tasks. During this phase the GNSS observations are validated using a statistic test, where multiple satellites can be rejected if needed. Following this validation, an integer ambiguity resolution method is applied to fix the carrier phase ambiguities following a confirmation step of the fixed values. At this point a second detection and exclusion strategy is used to keep only the ambiguities that were properly fixed. Once an optimal solution is obtained, the protection levels are computed, and the outputs are generated.

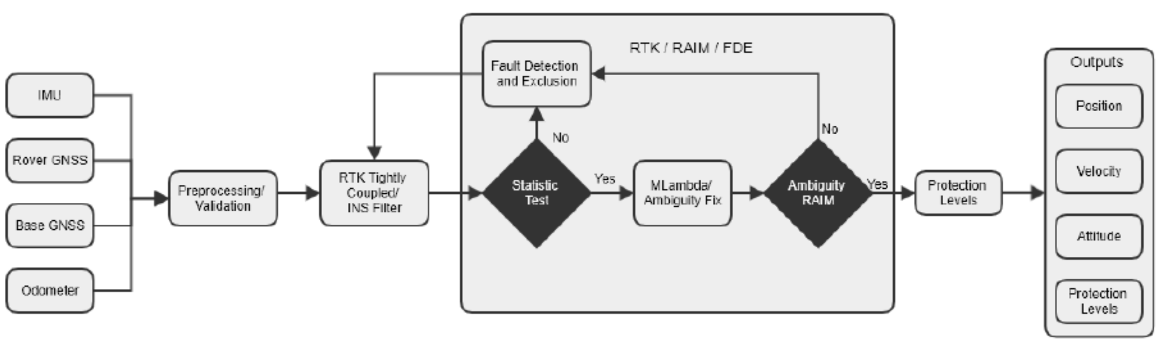

Figure 3: Integrity Overview.

2. Fault Detection and Exclusion

The FDE is generally based on the calculation of the residuals between the measurements and the Kalman prediction, as seen in Equation1.

$$\hat{r} = z - H\hat{x} \tag{1}$$

The FDE can be described as an iterative function that consists of two separate steps:

a) Global Test

The objective of this test is to check the consistency of the solution according to a predefined integrity risk and a statistical test that follows a Chi-squared distribution. The statistic test t in Equation 2 used is also knows as Normalized Sum of Squared Error (NSSE) [7], which can be expressed as:

$$t = \hat{r}^T W^{-1} \hat{r} \tag{2}$$

With:

$$W = H_k P_k^- H_k^T + R_k \tag{3}$$

Under fault-free conditions, the statistic test t follows a central χ^2 distribution. With a predefined probability of false alarm P_{fa} and a calculated redundancy, a threshold (Th) can be deduced, and the statistical hypothesis test can be conducted as follows:

$$\begin{aligned} H_0 &: \text{fault free conditions} \quad t \leq Th \\ H_a &: \text{faulty conditions} \quad t > Th \end{aligned} \tag{4}$$

In case the null hypothesis H_0 is rejected, and the alternative hypothesis H_a is accepted, then the fault identification procedure is needed to isolate and exclude the faulty measurement. The local test is the used method to release the fault identification.

b) Local Test

The rejection of the null hypothesis in the GT means that one or several measurements are faulty. The essence of fault exclusion is to survey for anomalies in all observations, and if a fault is detected, the corresponding measurement should be excluded.

The residual ($\hat{r}$) cannot be normalized simply by dividing the corresponding diagonal term of its covariance matrix S, due to the matrix S involves the cross correlations of the state components.The Cholesky decomposition is used to remove correlations [8], as shown in Equations 5 and 6:

$$S^{-1} = M^T M \tag{5}$$

$$\tilde{r} = M\hat{r} \tag{6}$$

An iterative process has been developed to identify and exclude faulty measurements. The valid measurement subset is then tested according to H_0 test to be validated, which ends with a valid navigation solution. In the case the number of measurements becomes too small, the solution is then declared as invalid.

3. EKF-Based Protection Level

The Protection Level (PL) is a statistical error bound (Figure 4), which characterizes the maximum allowed positioning error with probability derived from the integrity risk. It can be divided into horizontal (HPL) and vertical (VPL) components. In safety critical applications, it is necessary and even mandatory to meet the requirement $PL > PE$ (Position Error when the ground truth is known) and to ensure that PE is below a certain Alert Limit (AL). The AL is defined by a user according to its application requirements. Different algorithms for the PL computation can be found in the literature ([9], [10], [7]); A big focus on this paper was to select the algorithm that bounds the best the PE.

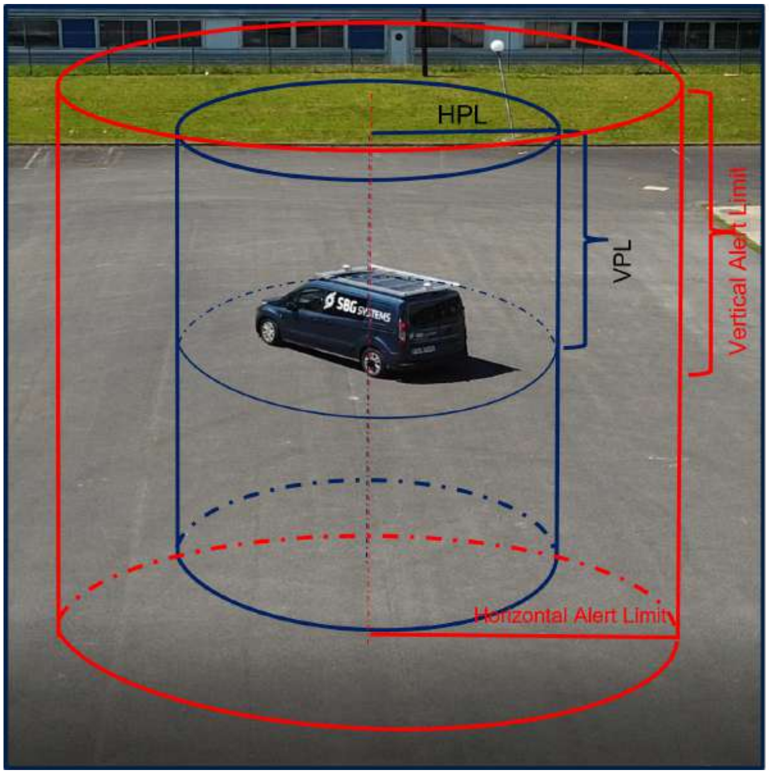

Figure 4: Protection Levels.

Several PL algorithms were tested, and the best performances were obtained using a combination of noise and bias PL as defined by [8]:

$$PL = PL_n + PL_b \tag{7}$$

For automotive application, we focus on the horizontal dimension only. In the following section, the formulas are expressed in relation to HPL, this is just a simplification as they are also valid for VPL.

a) Horizontal Protection Level Noise

Caused by the noise measurement, it is defined as:

$$HPL_n = K \times d_{major} \tag{8}$$

Where:

- K : inflation factor applied to meet the specified integrity risk.
- d_{major} : position uncertainty calculated as $d_{major} = \sqrt{P_{ee} + P_{nn}}$
- Pee, Pnn are the variance of the horizontal position from the covariance matrix P in NED.

b) Horizontal Protection Level Bias

Caused by the biased measurements, it is defined as:

$$HPL_b = max(H_{slope}) \times pbias \tag{9}$$

$$H_{slope} = \sqrt{\frac{(A_{1i}^2 + A_{2i}^2) * redundancy}{1 - B_{ii}}} \tag{10}$$

$$A = (H^t W H)^{-1} H^T W \tag{11}$$

$$B = HA \tag{12}$$

Where :

- pbias = $\sqrt{NSSE}$ = $\sqrt{t}$

IV. EXPERIMENTAL RESULTS AND ANALYSIS

1. Open Sky Scenario

The first scenario consists of an automotive test in an open sky environment. The trajectory followed during this test can be seen in Figure 5, it is clear that this rural area presents optimal conditions for the navigation system. The base station SBGS located at approximately 1 km was used for the RTK, in addition to an odometer and the corresponding automotive constraints for the application.

Two different configurations were under test. First, a GNSS only mode using an automotive grade multi-band receiver (Ublox ZED-F9P) in a RTK processing. Secondly, an industrial grade MEMS IMU (Ellipse-D) in an RTK tightly coupled IMU/GNSS/Odometer configuration. In order to generate a high precision reference for this specific test, a FOG based INS (Navsight Horizon) with odometer also in tightly coupled integration was used to compute a trajectory in a post processing algorithm in a FW/BW/Merge mode. The reference benefits from a 100 % fix rate.

Figure 5: Open Sky Scenario: Trajectory.

a) GNSS Results

As expected, the results under these ideal conditions are excellent, even in a GNSS only mode. Figure 6 shows the horizontal error of the position solution as well as the horizontal protection level. We can see that we obtain a centimeter precision and that the protection levels are consistent. The Stanford diagram for this test is presented in Figure 7, the solution is available and integer 100 % of the time, even as the alert limit chosen for this configuration was of only 1 m. Table 1 contains the horizontal errors and the protection levels for three different percentiles, in the most strict case the error is about 0.029 m with an HPL of 0.711 m.

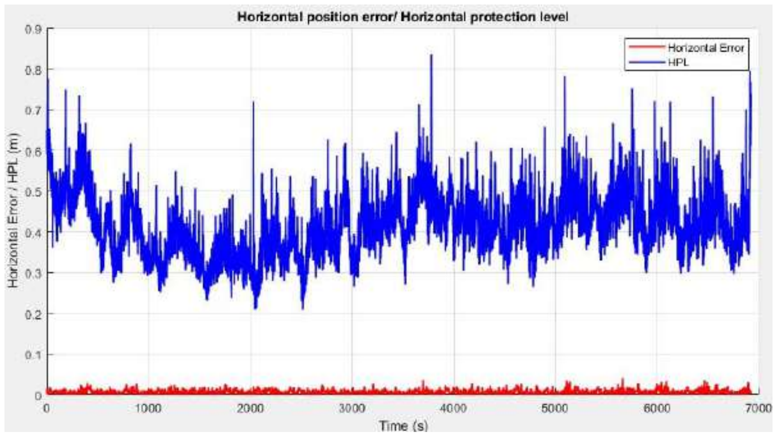

Figure 6: Open Sky Scenario: GNSS Horizontal Error.

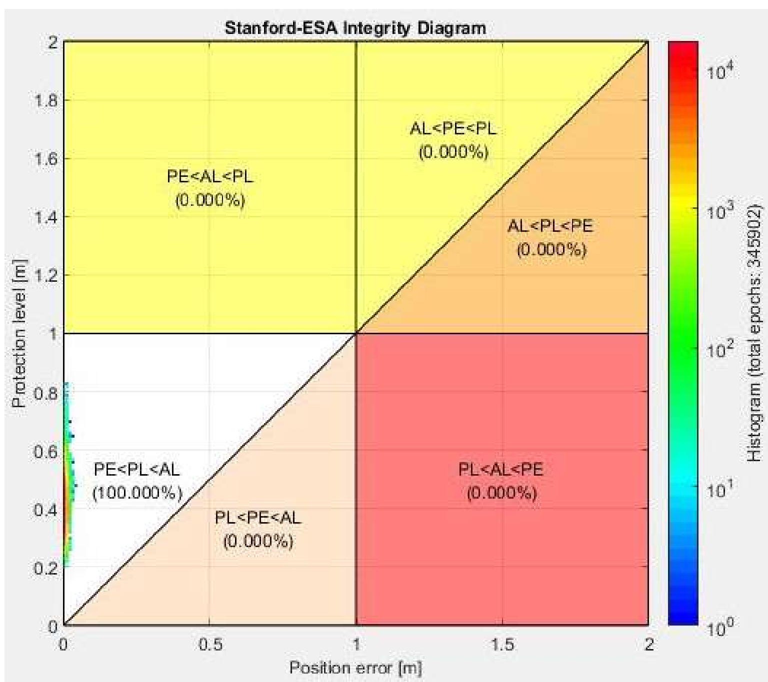

Figure 7: Open Sky Scenario: GNSS Stanford Diagram.

Percentile	68	95	99.7
Horizontal error (m)	0.009	0.017	0.029
HPL (m)	0.446	0.543	0.711

Table 1: Open Sky Scenario: GNSS Results

b) Tightly coupled INS/GNSS results

The conditions of this test are so optimal that the results of the GNSS only configuration can hardly be improved. In Figure 8 we can see the centimeter level precision of the tightly coupled solution, while the Stanford diagram shown in 9 emulates the previous results with an integer an available solution during the whole test. The overall results compiled in Table 2 estimate that the tightly coupled integration improves the GNSS solution, but by only a slight margin, which was expected.

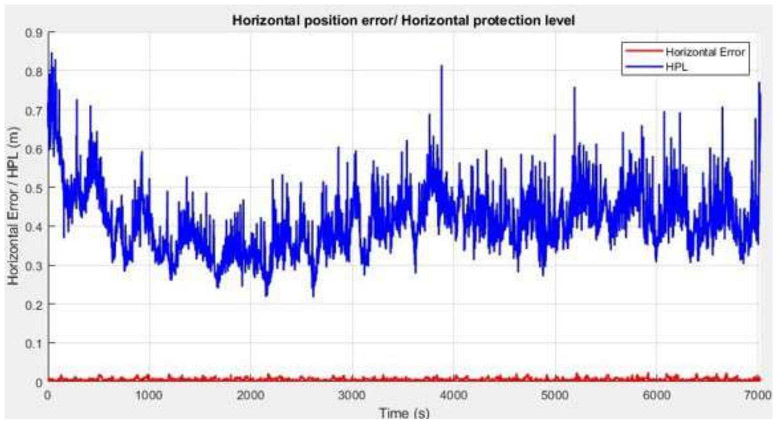

Figure 8: Open Sky Scenario: TC INS/GNSS Horizontal Error.

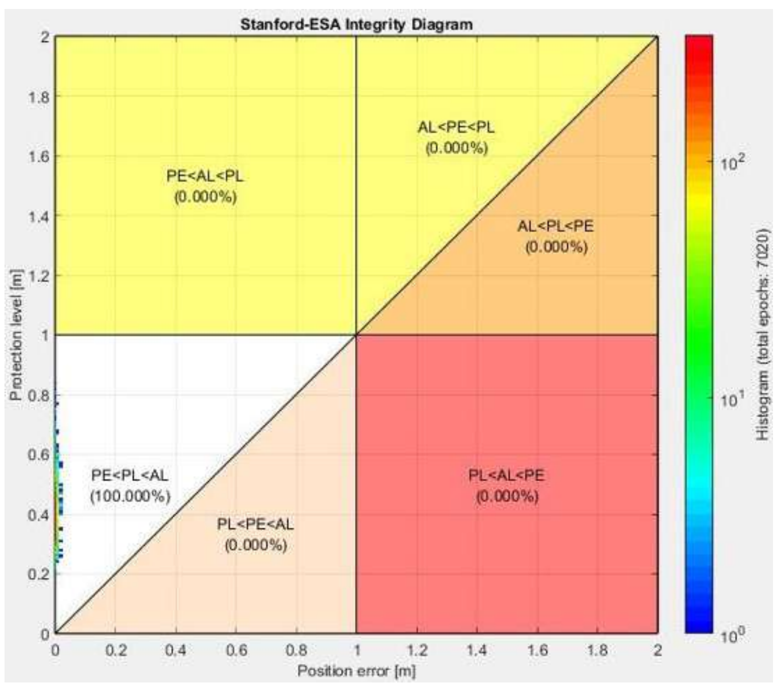

Figure 9: Open Sky Scenario: TC INS/GNSS Stanford Diagram.

Percentile	68	95	99.7
Horizontal error (m)	0.007	0.015	0.023
HPL (m)	0.444	0.536	0.645

Table 2: Open Sky Scenario: TC Results

2. Light Urban Scenario

The second scenario is more challenging from an integrity point of view. This automotive acquisition was made in a light urban area where the vehicle passed under a couple of bridges and the multi-path effects created by nearby buildings were more present. Regarding the RTK setup, there was a baseline of approximately 1 km between the rover and the base station and the constraints of an automotive motion profile were used. The same two devices are under test, on the one hand an automotive grade multi-band GNSS receiver for the GNSS only mode, and on the other hand an industrial grade MEMS INS fused with an RTK GNSS + odometer in a tightly coupled architecture. This case a Navsight Apogee, which is a survey grade INS, was used to compute the reference in a FW/BW/Merge post-processed algorithm.

Figure 10: Light Urban Scenario: Trajectory.

a) GNSS Results

For the GNSS only configuration the difficulties of the scenario are obvious. In Figure 11 we can see the horizontal error and the HPL, while Table 3 summarizes the performance of the system. Using the diagram in 12 we can clearly see that the quality of the solution is not perfect. In this case almost 10 % of the estimated solution is considered as unavailable, but the most important fact is that the solution never reaches the lower part of the diagonal of the diagram, where the systems become misleading and even dangerous. This kind of results are not enough for some safety of life applications such as the autonomous vehicle, under these light urban environments a solution that is available most of the time is needed.

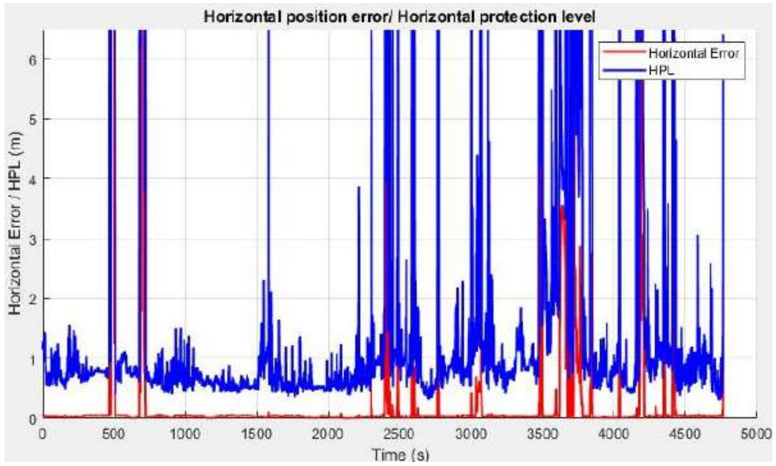

Figure 11: Light Urban Scenario: GNSS Horizontal Error.

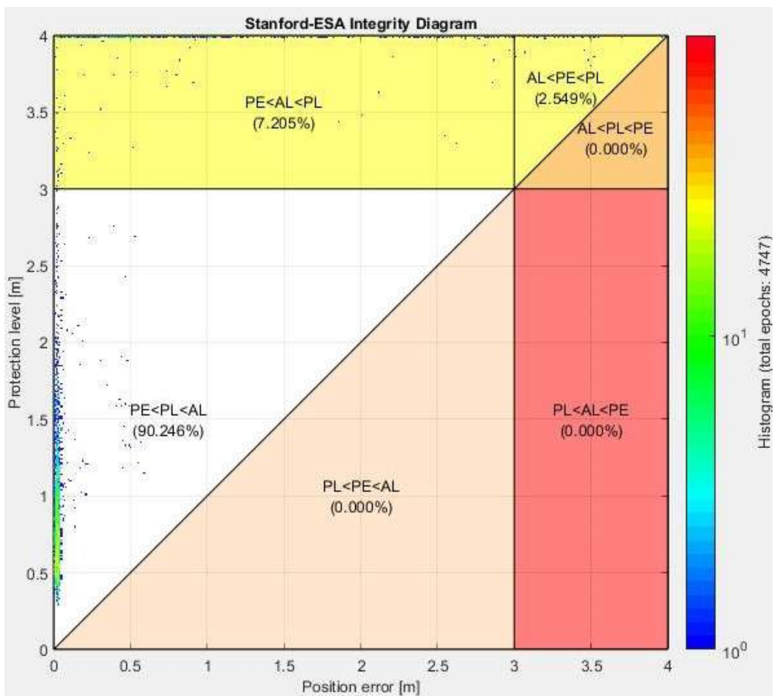

Figure 12: Light Urban Scenario: GNSS Stanford Diagram.

Percentile	68	95	99.7
Horizontal error (m)	0.036	1.003	107.54
HPL (m)	0.939	7.173	119.80

Table 3: Light Urban Scenario: GNSS Results

b) Tightly coupled INS/GNSS results

The tightly coupled implementation provides an important boost in the availability of the system. This time, Figures 13 and 14 show how the solution is available more than 96 % of the time. The rest of the epochs the system falls in the zone of not available, but it keeps the integrity for the totality of the test. Comparing Tables 3 and 4 we can clearly see the impact of the coupled architecture; the 99.7 percentile goes from 107.54 m in the GNSS only mode to 0.713 m in the tight implementation.

Another important note for this test is that the HPL for the 99.7 percentile are significantly high compared to the obtained horizontal error, some optimizations of the protection levels could be made in order to improve the availability.

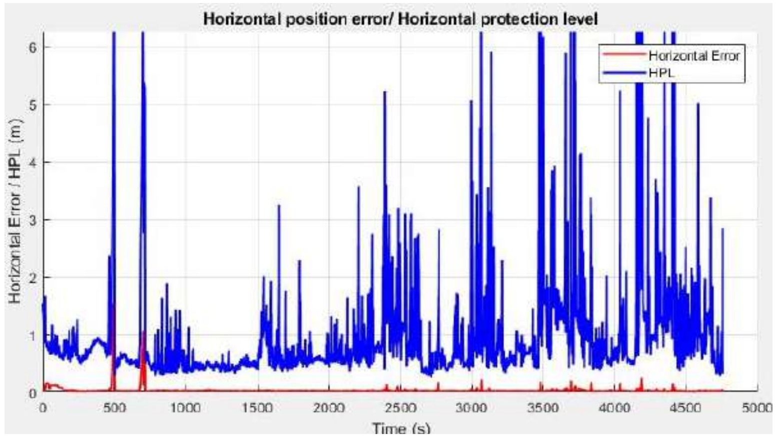

Figure 13: Light Urban Scenario: TC INS/GNSS Horizontal Error.

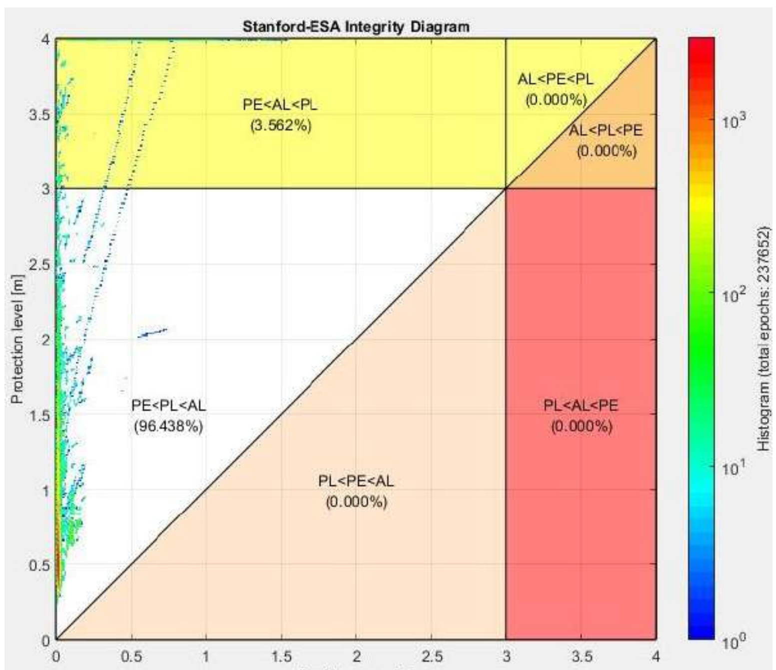

Figure 14: Light Urban Scenario: TC INS/GNSS Stanford Diagram.

Percentile	68	95	99.7
Horizontal error (m)	0.025	0.073	0.713
HPL (m)	0.863	2.345	11.764

Table 4: Light Urban Scenario: TC Results

3. Harsh Urban Scenario

The last scenario consists of a harsh urban environment, where the vehicle travels around the financial district of Paris. During this test not only the multi-path effects due to the number of high buildings is increased, but there are also multiple tunnels where the system is denied from any GNSS signal. Once again, two different configurations are tested, a GNSS only mode with an Ublox receiver and a tightly coupled MEMS INS / GNSS RTK mode. The reference is generated using a FOG based INS coupled with a GNSS receiver and an odometer in a FW/BW/Merge configuration.

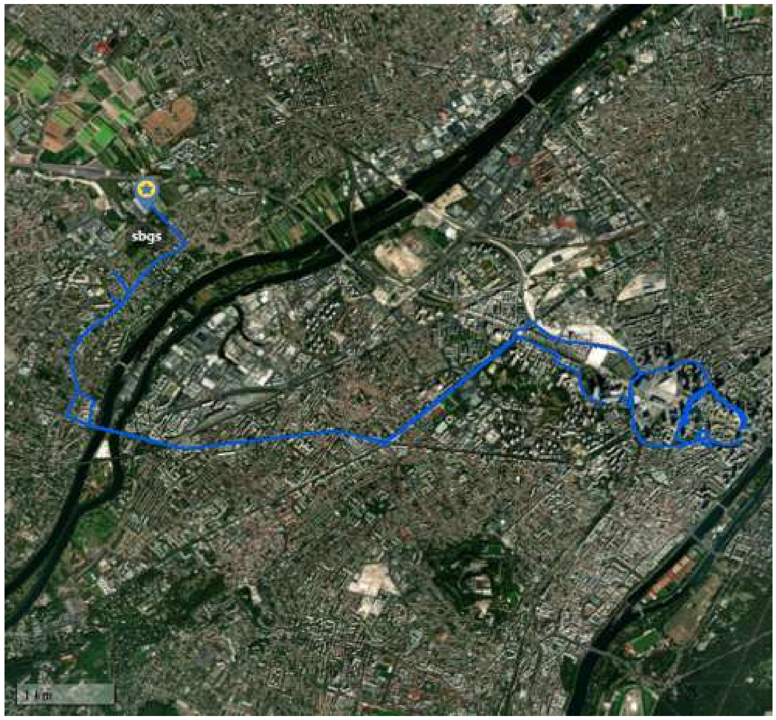

Figure 15: Harsh Urban Scenario: Trajectory.

a) GNSS Results

The GNSS only solution suffers from a lack of availability, this can be seen in Figure 17 were the Stanford diagram shows that only 60 % of the epochs produce an available solution. It is clear that the conditions have deteriorated the estimated position, however the results are kept on the upper diagonal of the diagram which is a requirement. Looking at the horizontal error in Figure 16 and Table 5 we can see that in such condition, the GNSS only solution is not able to reach a 68% error at a sufficient level for autonomous application.

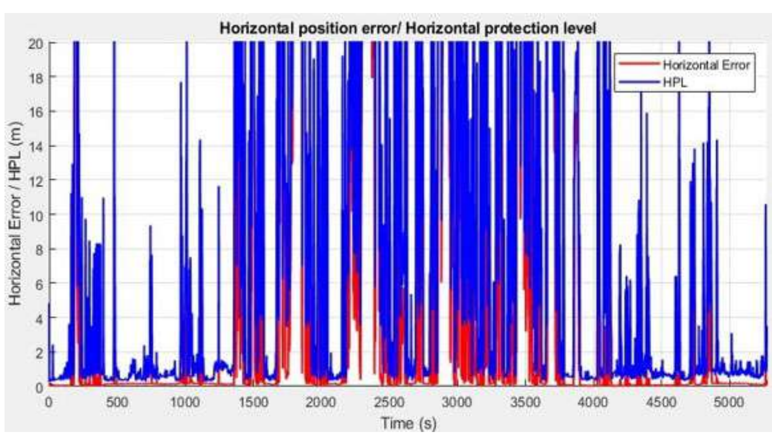

Figure 16: Harsh Urban Scenario: GNSS Horizontal Error.

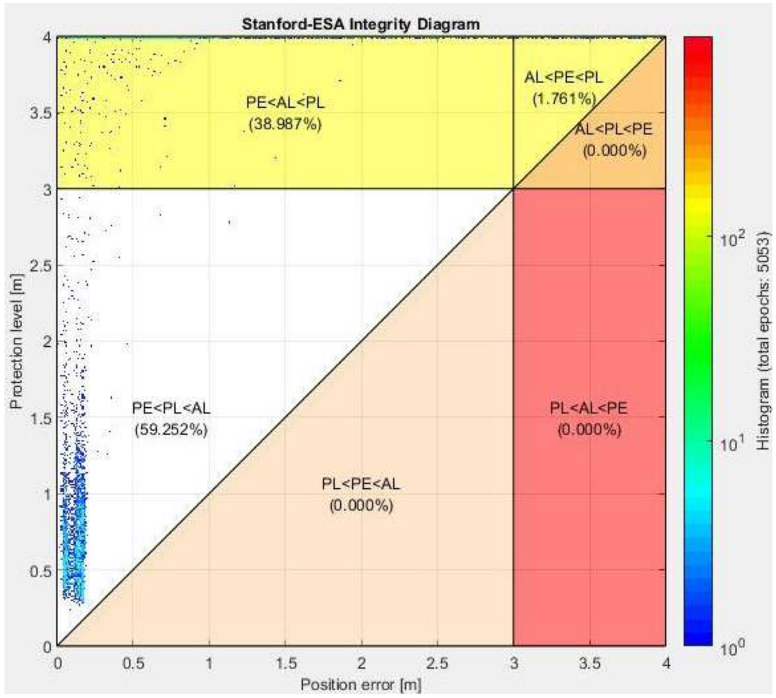

Figure 17: Harsh Urban Scenario: GNSS Stanford Diagram.

Percentile	68	95	99.7
Horizontal error (m)	0.489	47.43	237.82
HPL (m)	5.936	52.33	241.61

Table 5: Harsh Urban Scenario: GNSS Results

b) Tightly coupled INS/GNSS results

Compared with the previous results, the tightly coupled configuration greatly improves the availability and integrity of the solution. The additional sensors help to keep a consistent solution during some of the difficult periods of the acquisition, this is also reflected in the protection levels. As it can be seen in Figure 19 The solution is now available 72.5 % of the time, compared to 59.2 % in the previous configuration. These values may not be enough for a pure autonomous application, but the improvements found in the multi sensor solution cannot be neglected, especially considering the challenging environment of this test. An interesting finding is that the actual error at the 99.7th percentile is still under the 3 meters limit set in this test, although PL is at 63 m. This suggests that there could still be room for optimization in the system availability without changing the hardware. Additionally, to the Stanford diagram, the horizontal error and protection levels for the whole test are presented in Figure 18 with a compressed summary in Table 6.

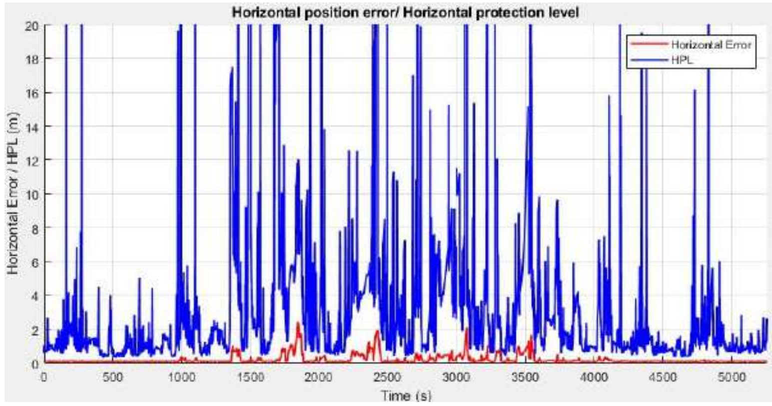

Figure 18: Harsh Urban Scenario: TC INS/GNSS Horizontal Error.

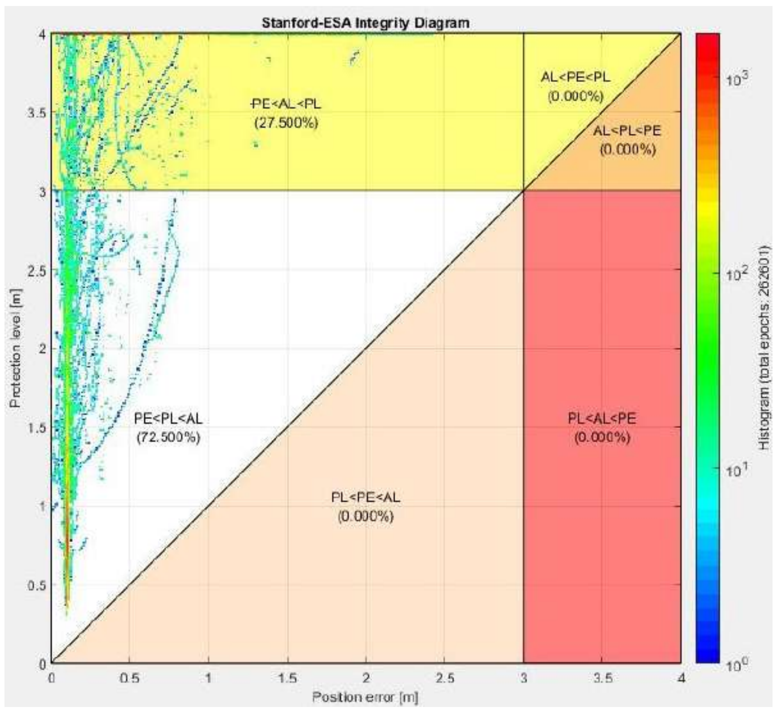

Figure 19: Harsh Urban Scenario: TC INS/GNSS Stanford Diagram.

Percentile	68	95	99.7
Horizontal error (m)	0.128	0.777	1.937
HPL (m)	2.52	10.514	63.966

Table 6: Harsh Urban Scenario: TC Results

V. CONCLUSIONS

The integrity algorithm presented in this article provides a reliable protection level that bounds the position error without any misleading information (MI), or hazardously misleading information (HMI) reported. Moreover, the integrity algorithm successfully detects and excludes all the faulty measurements which significantly improves the provided solution.

It has been proved that under open sky environments, both tightly coupled and pure GNSS algorithms provide a highly accurate solution with Protection Levels that bound the position error. However, under harsh urban environments, the multi-sensor fusion (GNSS, INS and Odometer) greatly improves the solution availability, accuracy and protection levels, this is even more noticeable during the partial or full GNSS outages.

REFERENCES

[1] G. Falco, G. Marucco, M. Nicola, and M. Pini, "Benefits of a tightly-coupled gnss/ins real-time solution in urban scenarios and harsh environments," 02 2017.

[2] I. Klein, S. Filin, and T. Toledo, "Vehicle constraints for supporting INS navigation in urban environments," *Navigation*, vol. 58, pp. 7–15, 03 2011.

[3] S. Vana, J. Aggrey, S. Bisnath, R. Leandro, L. Urquhart, and P. Gonzalez, "Analysis of GNSS correction data standards for the automotive market," *Navigation*, vol. 66, 07 2019.

[4] T. H. Tran and G. Belforte, "An ARAIM adaptation for kalman filter," *Workshop on Maritime Communication and Navigation (COMNAVI 2017)*, pp. 27–37, 12 2017.

[5] I. C. A. Organization", "Annex 10 aeronautical telecommunications," in *Convention on International Civil Aviation*, 6th ed. I.C.A.O, July 2006, vol. Volume I.

[6] O. Crespillo, A. Grosch, B. Belabbas, and M. Rippl, "GNSS-aided INS integrity concept," 09 2014.

[7] N. Zhu, D. Bétaille, J. Marais, and M. Berbineau, "GNSS integrity enhancement for urban transport applications by error characterization and fault detection and exclusion (FDE)," 12 2018.

[8] X. Han, A. Kazim, N. Ait Tmazirte, J. Marais, and D. Lu, "GNSS/IMU tightly coupled scheme with weighting and FDE for rail applications," 01 2020.

[9] J. Blanch, T. Walter, P. Enge, Y. Lee, B. Pervan, M. Rippl, and A. Spletter, "Advaced raim user algorithm description: Integrity support message processing, fault detection, exclusion, and protection level calculation," vol. 4, 09 2012.

[10] G. Gottschalg and S. Leinen, "Comparison and evaluation of integrity algorithms for vehicle dynamic state estimation in different scenarios for an application in automated driving," *Sensors*, vol. 21, p. 1458, 02 2021.